All-optical amplification in metallic subwavelength linear waveguides

Ramaz Khomeriki[1,2] and Jérôme Leon[3,*]

[1]*Max-Planck Institute for the Physics of Complex Systems, Nöthnitzer Strasse 38, 01187 Dresden, Germany*

[2]*Physics Department, Tbilisi State University, 0128 Tbilisi, Georgia*

[3]*Laboratoire de Physique Théorique et Astroparticules, CNRS-IN2P3-UMR5207, Université Montpellier 2, 34095 Montpellier, France*

(Received 12 February 2013; published 6 May 2013)

The proposed all-optical amplification scenario is based on the properties of light propagation in two coupled subwavelength metallic slab waveguides where, for a particular choice of waveguide parameters, two eigenmodes coexist: propagating (symmetric) and nonpropagating (antisymmetric). For such a setup incident beams realize boundary conditions for forming a stationary state as a superposition of the mentioned eigenmodes. It is shown both analytically and numerically that the amplification rate in this completely linear mechanism diverges for small signal values.

DOI: 10.1103/PhysRevA.87.053806 PACS number(s): 42.81.Qb, 42.60.Da, 42.79.Ta

Leading ideas in investigations of all optical logical devices in structured media [1] usually implement optical bistability [2] or soliton interaction [3] in creating the switching operation of optical beams. Quantum dots [4], single molecules [5], or atomic systems [6] could be also used for optically controlled switching of light. One can also quote various optoelectronic approaches [7] for the realization of optical transistors and asymmetric nonlinear waveguides for all optical diodes [8]. However, all the mentioned setups are based on nonlinear photon-photon interactions and hardly meet the criteria [9] for applicability in all-optical computing. Here we consider the possibility of amplification of optical signals using two subwavelength waveguides coupled by metallic film. The problem is linear with no need in high-power fields and there is a rich experience in the building of subwavelength photonic [10] and metallic waveguides [11].

Our idea of all-optical amplification is based on the possibility of the coexistence of two fundamental modes with real (symmetric mode) and imaginary (antisymmetric mode) wavenumbers along the longitudinal propagation direction of a dielectric-metal-dielectric combined waveguide system. In such a situation only the symmetric mode can carry nonzero flux, while the energy flux associated with the antisymmetric mode is exactly zero. Thus the propagation of the antisymmetric mode responsible for destructive interference is suppressed and the amplification effect can take place. Suggested effect is different than one in a homodyne receiver scheme, where signal intensity is amplified at the receiver area, while the total signal energy flux is not amplified. As we will show below, the total signal flux amplification is possible only in metallic subwavelength waveguides, where symmetric and antisymmetric modes are characterized by real and imaginary wavenumbers, respectively.

In principle, the suggested waveguide system could be of different geometries; in this paper we consider two dielectric slabs (with refractive index n) separated by a metallic film and we assume the perfect electric conductor (PEC) condition on both sides of the waveguide system. Thus the setup presented in Fig. 1(a) allows one to reduce the problem to 2 (space) + 1 (time) dimensions assuming the electric field is polarized and homogeneous along the y direction and having a fixed zero value at the boundaries. In nonmagnetic medium we can write down the following wave equations for the transverse electric field $E \equiv E_y$ perpendicular to the xz plane:

$$\Delta E - n^2 \partial_{tt} E = 0, \quad \Delta E - \omega_p^2 E - \partial_{tt} E = 0, \qquad (1)$$

where we work in the units $c = 1$ and use the definition $\Delta \equiv \partial_{xx} + \partial_{zz}$. The first equation in (1) corresponds to the wave propagation inside a dielectric, while the second equation describes the dynamics inside the metallic film in the approximation of zero Drude relaxation rate. Beyond this

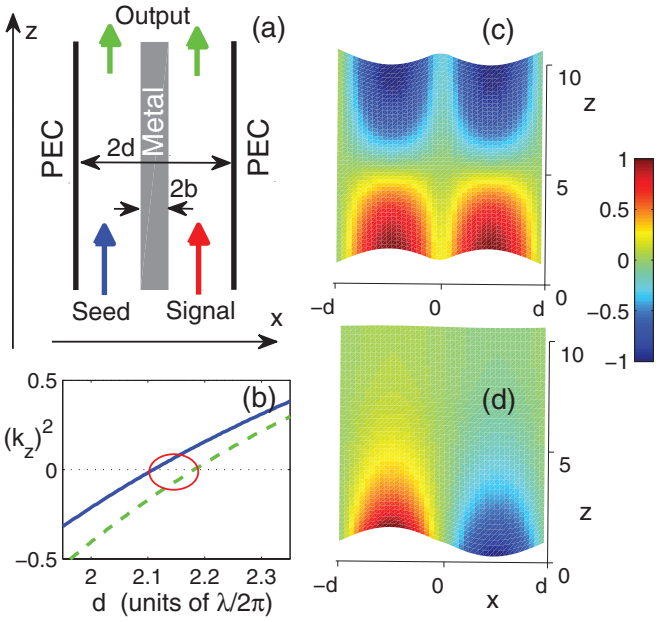

FIG. 1. (Color online) (a) Schematics for the dielectric-metal-dielectric waveguide system restricted by the perfect electric conductor (PEC) from both sides. (b) Dependence of the longitudinal wave number on the waveguide width d for two fundamental symmetric (solid) and antisymmetric (dashed) modes calculated from Eqs. (4) and (5); the thickness of the metallic film is fixed to the value $2b = 0.506(\lambda/2\pi)$. Panels (c) and (d) display snapshots for these modes according to expressions (6) and (7).

*Deceased.

approximation the electromagnetic wave dynamics inside the metal is governed by [12]

$$\Delta E - 4\pi\,\partial_t J - \partial_{tt} E = 0, \quad \partial_t J = -\frac{J}{\tau} + \frac{\omega_p^2}{4\pi} E, \qquad (2)$$

where J stands for the electric current density; $1/\tau$ stands for the Drude relaxation rate; $\omega_p = \sqrt{4\pi e^2 N/m}$ is a plasma frequency; and e, N, and m are charge, concentration, and mass of electrons, respectively.

For the sake of analytical simplification we assume negligible damping inside the metal ($\tau \to \infty$) getting from (2) automatically the initial system (1), and we work in the frequency range $\omega \ll \omega_p$ for which the metal is not transparent. Moreover, because of the placement of the PEC on both sides of the waveguide system, one has vanishing boundary conditions $E(x = \pm d) = 0$. Thus the stationary basic solution of (1) in the different parts of the combined dielectric-metal-dielectric symmetric waveguide system is written as follows:

$$\begin{aligned} E &= A \sin[k_x(d + x)]e^{i(k_z z - \omega t)} + \text{c.c.}, \quad -d < x < -b \\ E &= (F_1 e^{\kappa x} + F_2 e^{-\kappa x})e^{i(k_z z - \omega t)} + \text{c.c.}, \quad |x| < b \\ E &= B \sin[k_x(d - x)]e^{i(k_z z - \omega t)} + \text{c.c.}, \quad b < x < d, \end{aligned} \qquad (3)$$

where "c.c." means complex conjugated term and in the combined part of the waveguide one has a dielectric in the range $b < |x| < d$ and metal in the range $|x| < b$; A, B, F_1, and F_2 are real amplitudes of electric field in the dielectric and metallic parts, respectively; k_x is a real wave number in the dielectric; ω is a working frequency; and κ is the penetration depth in the metal. These wave numbers are linked by the dispersion relations

$$k_z = \sqrt{\omega^2 n^2 - (k_x)^2}, \quad \kappa = \sqrt{\omega_p^2 - \omega^2 + (k_z)^2}, \qquad (4)$$

which automatically follows putting solution (3) into wave equations (1). If we fix operational frequency ω and waveguide parameters b and d, all other quantities are uniquely defined. Particularly, from the continuity conditions of solution (3) at the lines $x = \pm b$, one gets the following relations for k_x:

$$\tan[k_x^{\pm}(d - b)][\tanh(\kappa b)]^{\pm 1} + [k_x^{\pm}/\kappa] = 0, \qquad (5)$$

where we have a $+(-)$ sign for the symmetric (antisymmetric) solution. Taking into account the dispersion relations (4), one can calculate $k_x^{\pm}$ and $k_z^{\pm}$ versus waveguide parameters b and d, and we are interested in the range of these parameters for which $(k_z^+)^2$ is positive while $(k_z^-)^2$ is negative [see Fig. 1(b) for the appropriate parameter values indicated by a circle]. Then defining the real quantities as $k_z^+ \equiv k_s$ and $k_z^- \equiv i k_a$ we can write the following for the symmetric and antisymmetric solutions:

$$E_s = \Phi_+(x)\cos(k_s z - \omega t); \quad E_a = \Phi_-(x)e^{-k_a z}\cos(\omega t), \qquad (6)$$

where orthogonal to each other the symmetric and antisymmetric profiles $\Phi_{\pm}(x)$ are defined as

$$\begin{aligned} \Phi_{\pm} &= \sin[k_x^{\pm}(d + x)], \quad -d < x < -b, \\ \Phi_{\pm} &= \frac{\sin[k_x^{\pm}(d - b)]}{e^{\kappa b} \pm e^{-\kappa b}}[e^{\kappa x} \pm e^{-\kappa x}], \quad |x| < b, \\ \Phi_{\pm} &= \pm \sin[k_x^{\pm}(d - x)], \quad b < x < d, \end{aligned} \qquad (7)$$

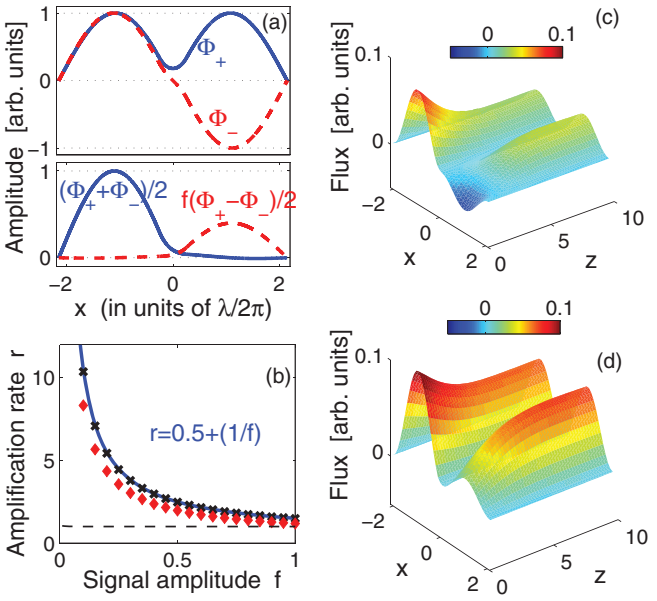

FIG. 2. (Color online) (a) The upper panel displays profiles of two fundamental modes given by Eqs. (7) and the lower panel presents their combinations which serve as a good approximation for boundary conditions of beams entering into the left (solid line) and right (dashed line) waveguides. (b) Results of numerical simulations (crosses) on acceleration rate versus signal amplitude f, which is compared with analytical formula (19) presented as a solid line. Panels (c) and (d) show energy flux density distribution within the waveguide system for signal amplitudes $f = 0$ and $f = 0.5$, respectively.

and we present snapshots of symmetric and antisymmetric solutions (6) in Figs. 1(c) and 1(d) while their profiles (7) along axis x and their combinations are presented in Fig. 2(a).

As long as the electric field has a single component along the transversal y axis one can readily compute the in-plane components of the magnetic field; particularly, H_x could be easily integrated form the Maxwell equation $\partial H_x/\partial t = \partial E/\partial z$. Then it is straightforward to calculate the energy flux density as $s_z = E H_x$ and the total energy flux along the longitudinal z direction as $S_z = \int_{-d}^{d} E H_x dx$. It is easy to see from (6) and (7) that averaged over time the total flux in the case of the symmetric eigenfunction is $\langle S_z^s \rangle \simeq dk_s/2\omega$, while in the antisymmetric case one has a standing wave profile along the z direction and consequently the averaged total flux $\langle S_z^a \rangle$ is exactly zero.

Now the question is which solution (symmetric or antisymmetric or their linear combination) is realized for the given boundary condition. Let us suppose that seed and input beams are injected from the isolated waveguides separated by the PEC. Thus we have the seed and input waveguides bounded by the PEC at $x = -d, 0$ and $x = 0, d$, respectively, and first of all we consider the symmetric incident field in the form of the following propagating wave at $z < 0$:

$$I_s = |\sin(\pi x/d)|\cos(k_s z - \omega t), \quad -d < x < d. \qquad (8)$$

This should be combined with the reflected beam with unknown amplitudes r_1 and r_2 characterizing the symmetric and antisymmetric contributions,

$$R = [r_1 \sin(\pi x/d) + r_2 |\sin(\pi x/d)|]\cos(k_s z + \omega t), \qquad (9)$$

and the sum $I + R$ should be connected with the linear combination $u_s E_s + u_a E_a$ of the solutions at $z > 0$ given by Eq. (6) via continuity conditions. Noting that in the case of narrow metallic films $b \ll d$ [see Fig. 2(a)] $\Phi_+ \simeq |\sin(\pi x/d)|$ and $\Phi_- \simeq \sin(\pi x/d)$, we easily get the condition $r_1 = r_2 = u_a = 0, u_s = 1$, meaning that there is no reflected wave and in a whole range of z and the symmetric solution is approximately given by

$$E = |\sin(\pi x/d)| \cos(k_s z - \omega t). \tag{10}$$

While in the case of the antisymmetric incident field the analysis is a bit more complicated, particularly, if we take the incident field in the form

$$I_a = \sin(\pi x/d) \cos(k_s z - \omega t), \quad -d < x < d, \tag{11}$$

from considerations similar to those above, we conclude that such a beam is completely reflected and a whole solution is written as follows:

$$\begin{aligned} E &= \sin(\pi x/d)\,[\cos(k_s z - \omega t) + \cos(k_s z + \omega t + \varphi)], \quad z < 0 \\ E &= u_a \sin(\pi x/d) e^{-k_a z} \cos(\omega t + \varphi/2), \quad z > 0, \end{aligned} \tag{12}$$

where $\tan(\varphi/2) = k_a/k_s$ and $u_a = 2/\sqrt{1 + (k_a/k_s)^2}$.

Now let us suppose that we have an incident seed beam entering into the left waveguide written in the form

$$E^I = \sin[\pi(x + d)/d] \cos(k_s z - \omega t), \quad -d < x < 0, \tag{13}$$

and $E^I = 0$ at the right part $0 < x < d$. Then it is clear that this beam before entering into the waveguide system carries the total averaged in time flux $\langle S_z^I \rangle = k_s d/4\omega$. At the edge of the waveguide system this seed beam realizes a boundary condition which could be approximately presented as a sum of symmetric and antisymmetric eigenfunctions (6) at the point $z = 0$ (note that all of those functions undergo the same time oscillations); thus we write [see also the bottom panel of Fig. 2(a)]

$$E^I(z = 0) \simeq \tfrac{1}{2}(E_s + E_a)|_{z=0}. \tag{14}$$

It is natural to expect that having such a boundary condition after some transient time the solution $(E_s + E_a)/2$ develops in a whole waveguide system as well and this is confirmed by our numerical simulations (please see below). Calculating the energy flux of this solution and taking into account that the flux of the antisymmetric solution is strictly zero, one gets half of the value of the incident averaged flux: $\langle S_z^I \rangle/2 = k_s d/8\omega$, meaning that only half of the intensity goes through the waveguide system and the rest is reflected back. A similar analysis holds for the signal field with amplitude f incident to the right waveguide in the form

$$E^f = f \sin[\pi(d - x)/d] \cos(k_s z - \omega t). \quad 0 < x < d, \tag{15}$$

and $E^f = 0$ for $-d < x < 0$; before entering the waveguide this beam carries the averaged total flux

$$\langle S_z^f \rangle = f^2 k_s d/4\omega, \tag{16}$$

which is a total gain of incident flux due to application of the signal. This signal beam also realizes a boundary condition at the right waveguide, but now it is given in the form $(f/2)(E_s - E_a)|_{z=0}$ [see again the bottom panel of Fig. 2(a)] and thus due to the presence of both seed and signal fields the following stationary solution develops in the waveguide system:

$$E \simeq \frac{(1 + f)E_s}{2} + \frac{(1 - f)E_a}{2}. \tag{17}$$

From arguments similar to those above that the antisymmetric mode is characterized by a zero averaged flux, it is obvious that such a field carries the averaged flux $\langle S_z^{\text{out}}(f) \rangle = (1 + f)^2 k_s d/8\omega$ and thus the total gain of the output flux due to the signal reads as

$$\langle S_z^{\text{out}}(f) \rangle - \langle S_z^{\text{out}}(0) \rangle = \frac{(2f + f^2)k_s d}{8\omega}. \tag{18}$$

This should be compared with the averaged over time input signal flux (16), and thus one gets the following for the amplification rate:

$$r = \frac{\langle S_z^{\text{out}}(f) \rangle - \langle S_z^{\text{out}}(0) \rangle}{\langle S_z^f \rangle} = \frac{1}{2} + \frac{1}{f}, \tag{19}$$

which diverges at small signal values. Next our aim is to confirm this analytical result by numerical simulations.

For this purpose we first derive the boundary-value data at the lines $z = 0$ and $z = L$ (L is a length of the system) following Refs. [13,14], which represent incident waves entering the combined waveguide from the seed and signal and going out. As we have mentioned above before entering the waveguide system the seed and signal fields are described by Eqs. (13) and (15); thus in the range $z \leqslant 0$ the solution reads

$$E = [I(x) \cos(k_s z - \omega t) + R(x) \cos(k_s z + \omega t)], \tag{20}$$

where one has the following for $I(x)$:

$$I(x) = \sin[\pi(d + x)/d] \quad \text{and} \quad I(x) = f \sin[\pi(d - x)/d] \tag{21}$$

for $-d < x < 0$ and $0 < x < d$, respectively, while $R(x)$ is an unknown amplitude profile for the reflected wave and thuse has to be eliminated. The continuity conditions at $z = 0$ with the electric field $E(x,z,t)$ inside the combined waveguide can be written as

$$\begin{aligned} [I(x) + R(x)] \cos(\omega t) &= (E)_{z=0}, \\ k_s[I(x) - R(x)] \sin(\omega t) &= (\partial_z E)_{z=0}, \end{aligned}$$

which can be combined to exclude the unknown reflected amplitude $R(x)$ taking the time derivative from the first equation and then combining the resulting one with the second equation. Similar manipulations could be done with the boundary conditions at $z = L$ but then there is no contribution of the backward propagating field; thus the resulting equations read as

$$\begin{aligned} \partial_z E|_{z=0} &= (k_s/\omega)\partial_t E|_{z=0} + 2k_s I(x) \sin(\omega t), \\ \partial_z E|_{z=L} &= -(k_s/\omega)\partial_t E|_{z=L}. \end{aligned} \tag{22}$$

Thus we solve numerically the initial equations (1) with the boundary conditions (22) and definition (21) for $I(x)$. Next we compute the averaged over time longitudinal flux density $\langle s_z \rangle$ inside the waveguide system and its total value $\langle S_z \rangle$ across

the system and compare the latter to the value of the total incident signal flux given by Eq. (16) for different values of signal amplitude f. Finally we compare numerical results with the analytical prediction (19). We choose the operational frequency ω such that the vacuum wavelength is $\lambda = 0.7\ \mu$m, as a dielectric we take glass with a refractive index $n = 1.5$, and we choose silver as a metal complex refractive index of which for the mentioned wavelength is $\tilde{n} = n_1 + in_2 = 0.05 + 5i$ [15]. Thus we can derive the plasma frequency needed in (1) as follows $\omega_p \simeq n_2\omega$ [16]. The width of the waveguide system is taken as $2d = 4.294(\lambda/2\pi)$ and the metallic film thickness is chosen as $2b = 0.506(\lambda/2\pi)$. For such a choice of waveguide parameters the wave number of the symmetric propagating mode is $k_s = 0.25(2\pi/\lambda)$ and this value is used in the boundary conditions (22). Measuring the total flux for various values of signal amplitudes we have plotted Fig. 2(b), which shows an excellent correspondence with analytical formula (19), while in Figs. 2(c) and 2(d) we plot the distribution of the averaged in time flux density for two values of signal amplitude: $f = 0$ and $f = 0.5$. Finally, in the Supplemental Material the time evolution animations of the electric field and associated flux densities are presented [17].

In conclusion, we present a mechanism of signal amplification based solely on linear effects and confirm the amplification scenario by numerical simulations. In principle the analysis could be extended in the case of a single waveguide with a metallic boundary when the seed is directly injected into the waveguide while the signal beam is illuminated from the metallic film side. The above studies could be generalized for different systems where propagating and nonpropagating fundamental modes coexist.

R.K. is indebted to S. Flach, F. Lederer, T. Pertsch, and A. Szameit for many criticisms and useful suggestions. This work is supported by a joint grant from CNRS and RNSF (Grant No. 09/08) and grant from SRNSF No. 30/12.

[1] R. Keil *et al.*, Sci. Rep. **1**, 94 (2011).
[2] H. M. Gibbs, *Controlling Light with Light* (Academic Press, San Diego, 1985); D. Chevriaux, R. Khomeriki, J. Leon, Modern Phys. Lett. B **20**, 515 (2006).
[3] R. McLeod, K. Wagner, and S. Blair, Phys. Rev. A **52**, 3254 (1995).
[4] I. Fushman *et al.*, Science **320**, 769 (2008).
[5] J. Hwang *et al.*, Nature (London) **460**, 76 (2009).
[6] H. Mabuchi, Phys. Rev. A **80**, 045802 (2009).
[7] A. L. Lentine *et al.*, IEEE J. Quantum Electron. **25**, 1928 (1989).
[8] S. Lepri and G. Casati, Phys. Rev. Lett. **106**, 164101 (2011).
[9] D. A. B. Miller, Nat. Photonics **4**, 3 (2010).
[10] O. Peleg, M. Segev, G. Bartal, D. N. Christodoulides, and N. Moiseyev, Phys. Rev. Lett. **102**, 163902 (2009).
[11] J. A. Porto, L. Martin-Moreno, and F. J. Garcia-Vidal, Phys. Rev. B **70**, 081402(R) (2004).
[12] N. W. Ashcroft and N. D. Mermin, *Solid State Physics* (Harcourt College Publishers, Fort Worth, TX, 1975).
[13] W. Chen and D. L. Mills, Phys. Rev. B **35**, 524 (1987).
[14] R. Khomeriki and J. Leon, Phys. Rev. A **80**, 033822 (2009).
[15] P. B. Johnson and R. W. Christy, Phys. Rev. B **6**, 4370 (1972); see also http://refractiveindex.info.
[16] M. Born and E. Wolf, *Principles of Optics* (Pergamon, London, 1965), Chap. 13.
[17] See Supplemental Material at http://link.aps.org/supplemental/10.1103/PhysRevA.87.053806 for time evolution animations of the electric field and associated flux densities.